AC Cascading Failure Model for Resilience Analysis in Power Networks

Matthias Noebels, *Student Member, IEEE*, Robin Preece, *Senior Member, IEEE*, and Mathaios Panteli, *Senior Member, IEEE*

***Abstract*—Cascading failures are one of the main mechanisms causing widespread blackouts of power networks. Models simulating the behavior of cascading failures are widely used in the literature to understand fault propagation and investigate effective mitigation strategies. However, there is a lack of validated models that address the specific requirements of resilience analysis in power networks and that are computationally fast and converge reliably for very large contingency sizes that may occur under extreme events. This article presents a novel comprehensive ac cascading failure model particularly designed for resilience analysis in power networks. The model is capable to deal with large contingency sizes, it is computationally efficient in large networks and integrates seamlessly with established resilience metrics. It incorporates dynamic phenomena and protection mechanisms using static representations. The model is verified following the recommendations by the IEEE PES working group on cascading failures using internal validation, sensitivity analysis, and comparison to historical outage data. Furthermore, an analysis of the impact of different contingency sizes and the dependency of cascades on network loading level, are given to illustrate some applications of the model and to highlight its capabilities.**

***Index Terms*—Cascading failures, power system faults, power system modeling, resilience.**

I. Introduction

TACKLING cascading failures, one of the main mechanisms causing widespread blackouts of the power network, have been widely recognized as a crucial aspect in increasing resilience to extreme weather events [1], [2]. A cascading failure is the uncontrolled and successive loss of parts of a power network, usually triggered by one or more disturbance events [3]. The propagation of cascading failures is facilitated by overloading, angular instability, voltage stability, and other conditions identified by the IEEE Task Force on Understanding, Prediction, Mitigation, and Restoration of Cascading Failures [4]. The identification and testing of effective mitigating strategies requires a deep understanding of how cascading failures are triggered and how they propagate. Resilience is, in terms of a power network, usually interpreted as the ability to "rapidly recover from such disruptive events, and adapt its operation and structure to prevent or mitigate the impact of similar events in the future" [5]. Cascading failure models play a crucial part in many resilience studies [5]–[7], and a large number of cascading failure models is reported in the literature. The work in [8] gives an overview of a broad range of approaches, and groups them based on their characteristics into topological models [9], stochastic simulation models [10], high-level statistical models [11]–[13], dynamic simulation models [14], [15], and other interdependent or specialist models.

Resilience analysis to extreme events requires cascading failure models that reliably converge and thus provide meaningful results even for large contingencies. Additionally, models often have to be applied to large datasets and networks and, therefore, need to be computationally fast. Dynamic models provide comprehensive details about cascades, but require extensive and often unavailable input data describing the dynamic characteristics of a power system. Additionally, dynamic models are often computationally expensive, which makes them impractical in large networks. dc-based models are, hence, frequently used in resilience studies [5], [7], [14], [16]–[18]. However, past outages have shown the significant role of voltage deviations and reactive power flows (PFs), such as during the 2003 blackout in the United States and Canada [19] or the 2009 blackout in Brazil [20]. While dc PF models are fast and numerically stable, they fail to incorporate these aspects. AC PF models usually suffer from nonconverging PFs, which regularly occur when considering stressed networks and large contingencies. Resilience analysis, however, depends on the analysis of such extreme conditions and thus requires dedicated cascading failure models. Some ac PF models, such as [21], do not address the matter of nonconverging PFs at all. Other models, such as [22], particularly address nonconverging PFs, but do not consider reactive power and voltage limits and lack subsequent reactions by protection mechanisms, such as excitation limiters and undervoltage load shedding (UVLS). These mechanisms play a crucial part in large cascading failures [4]. Additionally, resilience analysis requires a whole-systems approach, thus, models need to be able to link seamlessly to established resilience evaluation frameworks.

A further issue with current cascading failure models is a lack of a standardized validation procedure, which has been recognized by the IEEE PES working group on cascading failures [3]. As a result, the working group has identified a set of approaches that can be addressed when validating a cascading failure model.

1) Internal validation determines whether the modeling assumptions suit the aim of the model.
2) Comparing the model to real data overcomes the infeasibility of a complete internal validation.

Manuscript received June 16, 2020; revised September 4, 2020; accepted November 1, 2020. Date of publication December 4, 2020; date of current version March 24, 2022. The work was supported in part by the EPSRC through the Power Networks Centre for Doctoral Training under Grant EP/L016141/1 and in part by the Newton Prize project "Resilient Planning of Low-Carbon Power Systems" under Project 1304. *(Corresponding author: Matthias Noebels.)*

The authors are with the Department of Electrical and Electronic Engineering, The University of Manchester Faculty of Science and Engineering, Manchester M13 9PL, U.K. (e-mail: matthias.noebels@manchester.ac.uk; robin.preece@manchester.ac.uk; mathaios.panteli@manchester.ac.uk).

Digital Object Identifier 10.1109/JSYST.2020.3037400

3) A sensitivity study identifies modeling assumptions with significant impact on the outcome of the model.
4) Cross-validations against other models to understand the importance of different modeling assumptions.

There is a clear need for a cascading failure model that caters for the specific needs of resilience analysis and comprehensively addresses the validation approaches by the IEEE PES working group on cascading failures. The key contribution of this article is the formulation of a comprehensive ac cascading failure model (AC-CFM) in Section III, which is as follows:

1) specifically designed for resilience analysis by integrating seamlessly into established resilience metric frameworks;
2) stable for very large contingencies or extreme conditions by efficiently addressing convergence issues;
3) validated following the approaches by the IEEE PES working group on cascading failures;
4) compared to other ac-based models, explicitly incorporating dynamic phenomena such as voltage and frequency protection mechanisms in a static representation;
5) computationally faster than dynamic cascading models.

Section II describes the role a cascading failure model plays within multiphase resilience evaluation frameworks. Validation of the model is performed in Sections IV–VII, and demonstrations in Section VIII show the capabilities of the model for resilience analysis. Section IX concludes this article.

II. Resilience Evaluation Frameworks

The growing impact and frequency of power outages in the last decades underlines the rising need for power network resilience. Evaluating resilience to extreme events is an ongoing issue in recent literature [23], [24]. This becomes particularly important when assessing resilience in a whole-systems approach considering infrastructure interdependencies [25]. Many frameworks have been developed to address the multifarious processes involved in such events, with [26] giving an overview over different approaches. Of particular interest are multiphase frameworks, which separate the course of events into distinguishable stages [27], [28] as follows.

1) In the *predisturbance stage*, preparatory or preventive measures can be applied in face of an upcoming event.
2) In the *disturbance stage*, the network is hit by an external shock and its operation reduces.
3) The *degraded stage* marks the lowest operational state once the disturbance does not increase any more.
4) In the *restorative stage*, power network operation is restored until it reaches its predisturbance level.
5) In the *postrestoration stage*, the network can adapt to future events based on findings from past events.

The development of power network operation can be illustrated using a resilience trapezoid (see Fig. 1) [1], [27], [28]. Each of the stages requires a comprehensive assessment of the processes involved and forms the basis of its very own field of research, and individual models exist for each phase, such as restoration [29]–[31]. The objective of the model presented in this article is to provide a deep understanding of the disturbance stage of large power outages, whilst linking seamlessly to the other stages of resilience assessment. By combining the model presented in this article with models for the other event phases, an overall resilience evaluation can, thus, be undertaken. The integration into an established resilience framework is demonstrated in Section III-E.

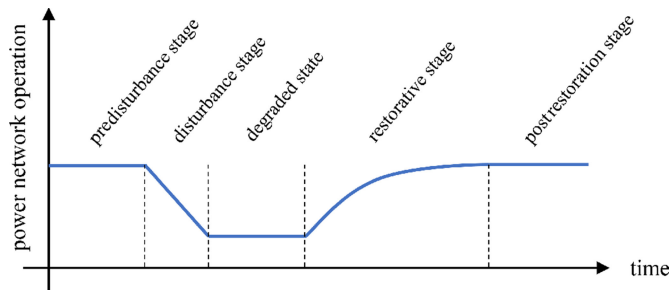

Fig. 1. Resilience trapezoid.

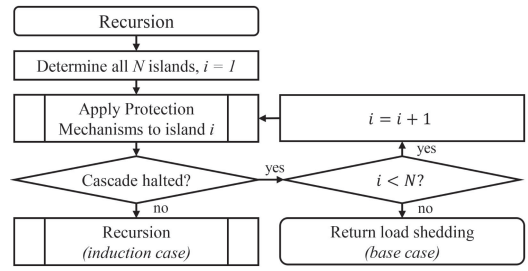

Fig. 2. Flowchart illustrating the recursive approach of AC-CFM.

III. AC Cascading Failure Model

This section describes the implementation of AC-CFM and presents an internal validation of the modeling assumptions by performing dynamic simulations.

AC-CFM is implemented[1] in MATLAB and uses the PF solvers of the MATPOWER toolkit [32]. The reference also contains the mathematical descriptions of the solvers. The model requires a MATPOWER network case structure and the initial contingency set as inputs. Any network component modeled in MATPOWER, i.e., buses, generators, loads, lines, transformers, and shunt devices, can be a part of the initial contingency set. The size of the initial contingency set is not limited, as it is with other models [16], [33].

A. Recursive Application of Protection Mechanisms

A cascading failure is governed by successive activation of protection mechanisms. This can cause disintegration of the network into islands, in which case the cascade may continue within each island independently. Most steady-state cascading failure models use iterative approaches to detect the islands at any discrete cascade generation and apply the necessary protection mechanisms. However, iterative approaches fail to identify causalities between generations and cannot address different time scales of protection mechanisms, because cascade generations are determined for the entire network even if it has disintegrated into independent islands. Instead, AC-CFM uses a recursive approach (see Fig. 2) to handle cascades within each island individually until the cascade comes to a halt. Beginning with the initial network, the PF within every island is calculated and protection mechanisms are applied (see Fig. 3). The protection mechanisms are explained in detail in Section III-C. If the protection mechanisms have changed the conditions within an island, such as loads, generators, or operating lines, the recursion is applied to the island again (induction case). If the conditions

[1]Source files are at https://github.com/mnoebels/AC-CFM

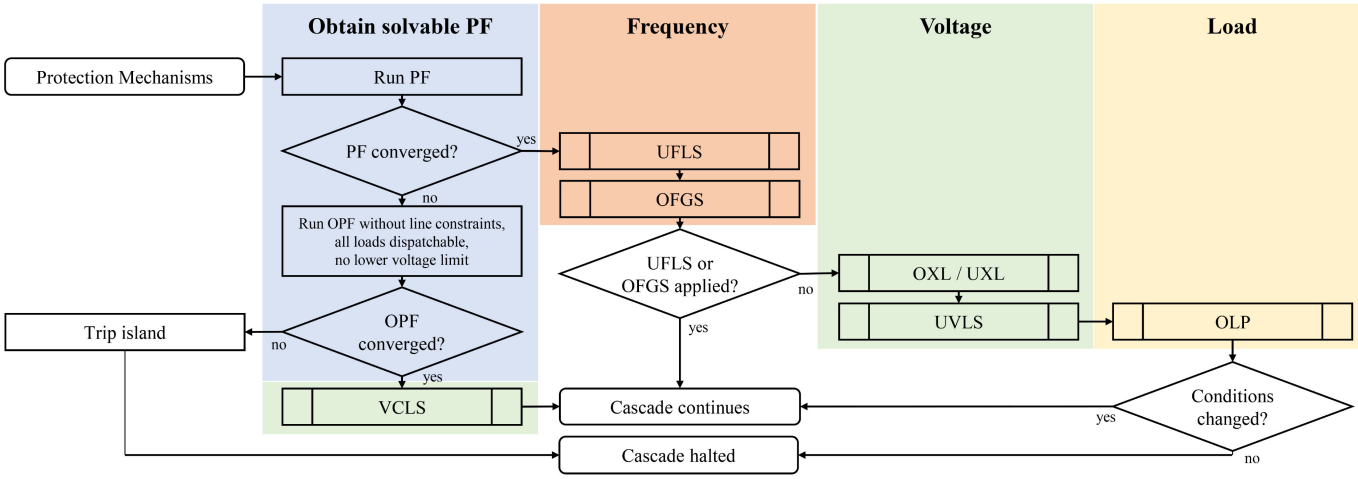

Fig. 3. Flowchart illustrating the implementation and succession of protection mechanisms in AC-CFM.

have not changed or are within the specified tolerances, the cascade within the island comes to an end, and the model proceeds with the next island (base case). This implementation is a tree traversal, depth-first search, in which the cascade in one island is handled until its termination before continuing with the next island.

Fig. 3 illustrates the succession of protection mechanisms in AC-CFM. Protection mechanisms require knowledge of the generators and loads as well as bus voltages and line currents. The initial step in the routine, therefore, is to obtain a solvable AC PF (see Section III-B). Afterward, protection mechanisms are applied (see Section III-C).

B. Obtaining a Solvable PF

A common problem when performing ac contingency analysis is that the ac PF solver may not converge. Nonconvergence is mainly a mathematical issue, as the PF equations do not provide a mathematical solution for the physical state the network is in. In some cases, this indicates that the network is beyond its physical capability. For instance, if the reactive power demand in a network is significantly larger than the reactive power generation capacity, a voltage collapse occurs. In a real power network, this would lead to undervoltage at some buses. If an UVLS scheme exists, loads would automatically be shed to support voltages. A cascading failure model needs to overcome unsolvable PFs by moving the system back into a solvable region, usually by shedding some loads. Previous models have addressed this either by assuming that nonconvergence leads to a blackout of the entire system, load shedding at all buses [34], reverting to a dc PF [35], or sensitivity factors identifying the loads that move the system most effectively back into the solvable region [22]. The challenge is to minimize the required load shedding, because this load shedding is a purely mathematical way of obtaining a solvable PF and does not correspond to any response of an actual power network. Furthermore, excessive load shedding may prevent the revelation of underlying voltage issues.

AC-CFM converts, in case of a nonconvergence, all loads to being dispatchable and uses an optimal power flow (OPF) solver to identify the minimum load shedding required to make the PF solvable again (voltage collapse load shedding, VCLS). Different established OPF solvers, such as MIPS [32] or IPOPT [36], can be integrated into AC-CFM, which further increases the range of solvable OPFs. Line and lower voltage limits are, at this point, disabled to not mathematically constrain the solution space. Loads in the island are then shed according to the OPF result and voltages at generating buses are set as calculated by the OPF. Often, VCLS leaves the network in a state with undervoltage at some buses or load violations. The modeling of subsequent protection mechanisms, hence, continues as usual (see Fig. 3). In rare cases, OPF does not converge even if all loads are reduced to zero, usually for small islands where reactive line losses exceed the available reactive power capacity. The island is then assumed to be beyond its physical capability and is tripped. Further elaboration on cases with nonconverging OPF is given in Section VI. The superiority of this approach is demonstrated in a cross-validation in Section VII.

C. Implementation of Protection Mechanisms

The different stages and implementations of protection mechanisms are explained in detail in the following sections. First, frequency stability is maintained. Second, over- and underexcitation are resolved and resulting undervoltages are handled. Third, lines exceeding their load rating are tripped by overload protection (OLP). Dynamic simulations, performed using DIgSILENT POWERFACTORY 2019 SP3 on the IEEE 39-bus test network, are used to internally validate the implementation of the individual mechanisms.

1) Under- and Overfrequency: When considering synchronous generators, sudden mismatches between electrical and mechanical power, for instance caused by unintentional islanding, result in a change in rotor frequency. Protection schemes such as underfrequency load shedding (UFLS) or overfrequency generator shedding (OFGS) can reestablish a balance of mechanical and electrical power and ensure that frequency stays within limits. For instance, standards by the North American Electric Reliability Corporation (NERC) require UVLS schemes to be capable of handling mismatches of up to 25% of the connected load [37]. Generator protection must be coordinated to prevent excessive shedding.

Algorithms 1 and 2 describe how UFLS and OFGS are implemented in AC-CFM. The maximum generation imbalance $\delta G_{\max}$ reflects the limited ability of generators to quickly adjust

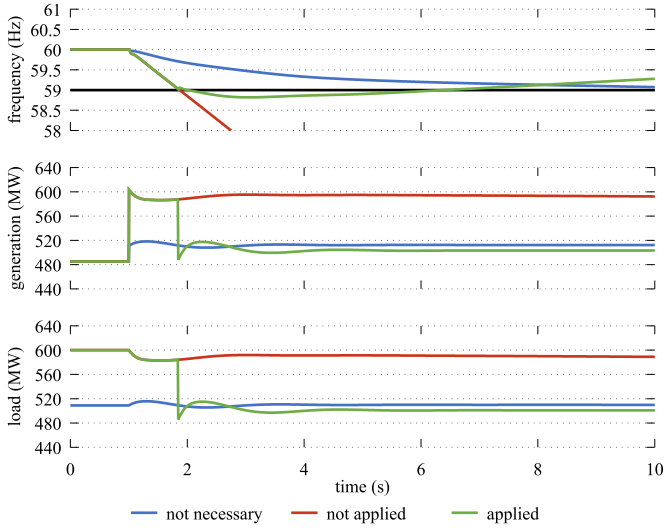

Fig. 4. Dynamic modeling of UFLS.

Algorithm 1: UFLS.

1: **if** generation increased by less than $\delta G_{\max}$ but does not exceed the available capacity **then**
2: Distribute slack generation so that it is shared by each generator proportional to its capacity whilst no generator exceeds its capacity.
3: **else**
4: Reduce loads to $(1 - \delta G_{\text{overhead}})$ of the previously dispatched generation increased by $\delta G_{\max}$, but not exceeding the available capacity.
5: **end if**

Algorithm 2: OFGS.

1: **if** generation decreased by less than $\delta G_{\max}$ **then**
2: Distribute slack generation so that it is shared by each generator proportional to its capacity whilst no generator exceeds its capacity.
3: **else**
4: Trip generators, beginning with the smallest, so that the dispatched generation does not exceed the total load by more than $\delta G_{\max}$.
5: **end if**

to load changes before the frequency exceeds the set limits. The dispatch overhead $\delta G_{\text{overhead}}$ caters for network losses. Assuming a single network frequency, UFLS sheds the same percentage of load at every bus, but prioritization of load shedding can be implemented in the proposed algorithm. Coordination of OFGS is done so that shedding starts with the smallest connected generator, for instance, because those are most likely to lose synchronism. UFLS and OFGS are repeatedly applied in the model until $\delta G_{\max}$ is no longer exceeded and a balance is established. In the model, it is assumed that frequency returns to nominal between cascade generations, i.e., that there is sufficient time for automatic generation control to act between successive trips of lines.

To demonstrate the behavior of the UFLS protection scheme, Fig. 4 shows the frequency response and connected active generation and demand of an island with insufficient generation that

Algorithm 3: OXL / UXL.

1: Determine all generators exceeding their reactive power limits as defined in the MATPOWER case structure.
2: Convert the buses of these generators to PQ buses.
3: Set their reactive power output equal to their closest reactive power limit.

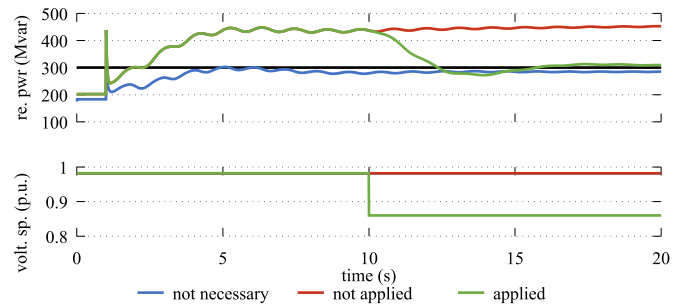

Fig. 5. Dynamic modeling of OXL.

has been disconnected from the network at $t = 1$ s. After islanding, the electric active power generation steps up significantly in order to meet the demand, which leads to a decreasing system frequency. If the imbalance between generation and demand is only small, the frequency stabilizes within the allowed frequency range (solid blue). If the imbalance between generation and demand is large, the frequency decreases gradually and will exceed the allowed frequency range eventually (dashed red). In this example, reducing the load by 17% lets the frequency return to the allowed range (dotted green).

2) Over- and Underexcitation: If the reactive power demand from a generator changes, its excitation system reacts by adjusting the excitation voltage in order to keep the terminal voltage stable. While the excitation system can adjust the field within a certain range to cater for different reactive power outputs, over- and underexcitation leads to overheating and eventually damage to the generator, and needs to be prevented. Over- (OXL) and underexcitation limiters (UXL) constrain the field current, and as a result the terminal voltage is adjusted.

The implementation of OXLs and UXLs in AC-CFM is shown in Algorithm 3. In ac PF, buses are either specified as PV (active power and voltage) or PQ (active and reactive power) buses, identifying which are the fixed parameters at the bus. Demand buses are generally PQ buses, while generating buses are usually PV buses. In Algorithm 3, buses with generators that exceed their reactive power limits are converted to PQ buses, meaning that their reactive power output is now fixed to its closest, upper or lower reactive power limit, and the bus voltage now becomes variable. This effectively mimics the impact of OXLs and UXLs.

The behavior of an OXL is demonstrated in Fig. 5. After a line fault at $t = 1$ s and subsequent islanding, the reactive power output of the shown generator increases. Depending on the demand, the reactive power output can be within the reactive power limits of the generator (solid blue) or outside (dashed red). In order to prevent the generator from damage, the OXL effectively reduces the terminal voltage of the generator after a time delay ($t = 10$ s, dotted green). While actual implementations of OXLs and UXLs differ and act on different components of the generator, Fig. 5 illustrates in simple terms how overexcitation can successfully

Algorithm 4: UVLS.

Shed δP_{ls} of load at buses falling below the UVLS trigger voltage U_{UVLS}.
if applied load shedding at a bus exceeds $\delta P_{\text{ls,max}}$ **then**
  Trip all loads at this bus
end if

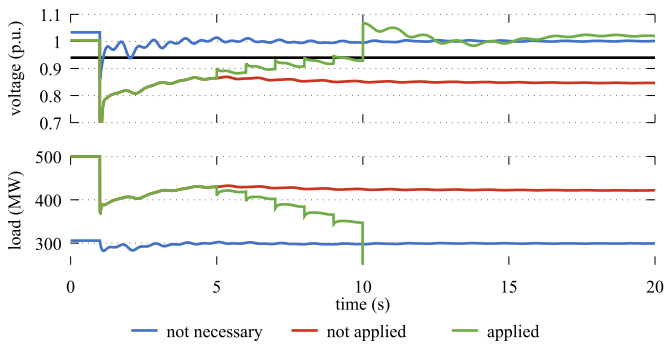

Fig. 6. Dynamic modeling of UVLS.

be prevented. If the terminal voltage exceeds the voltage limits after triggering the OXL, UVLS can be applied, which is part of Section III-C3.

3) Undervoltage: Reactive PF leads to a voltage drop at the receiving end of a line. In order to prevent voltages below the lower voltage limit, UVLS can be applied, which gradually decreases the demand at the bus until the voltage is again within limits. UVLS is usually applied in blocks of predefined sizes. Algorithm 4 shows the implementation of UVLS in AC-CFM. The load shedding block size is defined as δP_{ls}, and the maximum block-wise load shedding before shedding all loads at the bus is $\delta P_{\text{ls,max}}$.

Fig. 6 demonstrates the behavior of UVLS, in which a line fault at $t = 1$ s and subsequent islanding causes a voltage drop at one bus. Depending on the reactive power demand at the bus, the voltage at the bus can stay within limits (solid blue) or outside (dashed red). With UVLS, 5% of load is shed at $t = 5, 6, 7, 8, 9$ s (dotted green). As the voltage is still below the lower voltage limit, at $t = 10$ s all loads at the bus are shed as a final measure to reestablish acceptable voltages.

4) Overload: The OLP in AC-CFM trips all lines that exceed their rating as defined in the MATPOWER case structure. This is to prevent lines from damage due to overheating and ensure safe operation. In real OLP, there is usually a time delay to allow short overcurrents. However, as AC-CFM does not model with respect to time, this is not necessary to model.

D. Cascade Visualization

AC-CFM provides a novel way of visualizing cascading failures as a tree-like graph (see Fig. 7). The graph expresses causalities in cascading failures and helps mitigating the impact of large and wide-spread blackouts. It holds all model output parameters, including the succession of protection mechanisms, the available loads, generators and lines, the disintegration of the network into islands, and the amount of load shedding at each generation. It can easily be accessed and searched by subsequent analysis procedures depending on the requirements

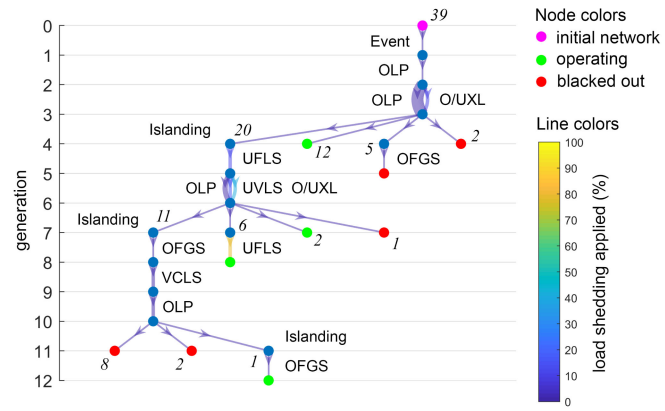

Fig. 7. Visualization of a cascade in the IEEE 39-bus network. Each circle represents the network or a part of it at a certain generation, starting with the initial network, and leading to four operating islands and five blacked-out islands. The number at each island gives the number of buses within the island. The connecting lines represent the protection mechanisms that have been applied between generations. The thickness of the lines indicate how many components have been affected, while the color indicates the percentage of load shedding.

TABLE I
VARIABLES EXTRACTED FROM THE RESILIENCE TRAPEZOID

Variable	Unit	Meaning
R_0	same as indicator	pre-disturbance resilience state
R_{pd}		post-disturbance resilience state
t_e	cascade generation	time of event
t_{ee}		time of the end of the event

of the researcher, even for very large networks or contingencies with thousands of buses and lines.

The example in Fig. 7 shows, beginning with a fully connected network and a single line fault, how a network first disintegrates into four islands due to OLP. After that, the protection mechanisms in each island try to stabilize frequency and voltage. At the end, each island either remains alive or blacks out. The full model output is shown in the Appendix. The graph reveals how the overloading of a single line triggers the entire cascade after the initial contingency. Reducing the loading of such critical lines or increasing their capacity can, for instance, prevent major blackouts. The graph can, thus, be used to identify key mechanisms that are crucial in the propagation of a failure cascade.

E. Integration Into Resilience Metric Frameworks

The straightforward and seamless integration with established resilience metrics enhances comparability and applications of AC-CFM to existing works and is a main advantage over other models, which have not addressed this need. The ΦΛΕΠ framework [27] will serve as an example for such an integration in this study. The framework provides a way of describing the shape of the resilience trapezoid [1], [27], which is the visualization of a resilience indicator R over time. The following indicators are used in this study: lost load, lost lines, lost buses, and lost generators. Fig. 8 shows the lost load in a network for an exemplary cascade triggered at $t = 0$. From the resilience trapezoid, the variables shown in Table I can be graphically extracted.

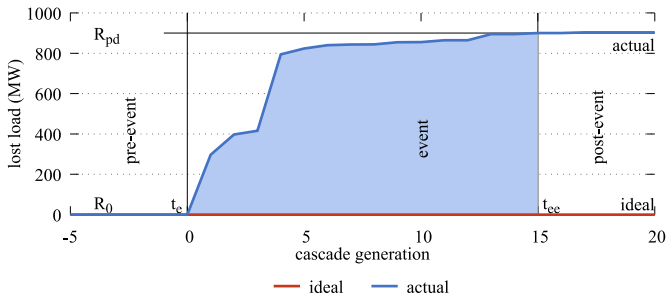

Fig. 8. Lost load over cascade generation with actual and ideal performance.

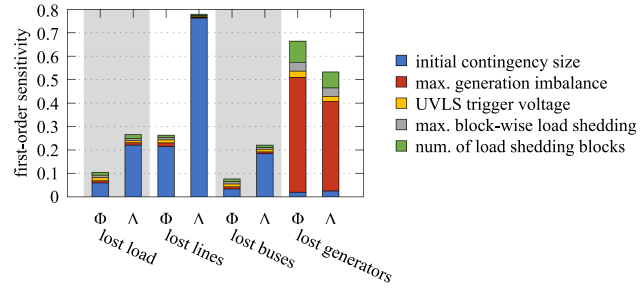

Fig. 9. First-order sensitivity coefficients calculated by FAST (missing values to one are higher order interactions).

TABLE II
CALCULATION OF THE Φ AND Λ RESILIENCE METRICS

Metric	Calculation	Unit	Meaning
Φ	$\frac{R_{pd}-R_0}{t_{ee}-t_e}$	indicator/ generation	How fast does resilience drop?
Λ	$R_{pd}-R_0$	indicator	How low does resilience drop?

Table II defines the Φ and Λ metrics from the ΦΛEΠ framework and how they are calculated based on the extracted variables. For the cascade in Fig. 8, $\Phi = 60$ MW/generation and $\Lambda = 900$ MW. As AC-CFM does not provide any information about the restoration after the cascade, only the Φ and Λ metrics from this framework can be calculated. The E and Π metrics can be obtained by feeding the postcascade network as calculated by AC-CFM into existing restoration models such as [30].

AC-CFM does not provide any timings for the cascade generations. The delay between cascade generations is a stochastic process and can, thus, not be calculated in a deterministic model. Instead, the discrete cascade generation is used as a timescale in the following. It should be noted that the timescale is, therefore, not linear and the actual time difference between two timesteps may vary.

IV. Sensitivity Analysis of Input Parameters

In the following, a sensitivity analysis for the model input parameters is performed, following the validation recommendations by the IEEE PES working group on cascading failures. Sensitivity analysis is done using a Fourier amplitudes sensitivity test (FAST) [38]. FAST calculates the first-order sensitivity coefficients that describe to what percentage the variance of model output parameters is related to the input parameters. FAST is a global sensitivity test, meaning that the sensitivity of an input parameter is averaged over variations in the other input parameters. Higher orders, i.e., interactions between input parameters, are ignored. For input parameters that show a large impact on the model output parameters, Spearman's rank correlation coefficient is calculated to identify whether there is a monotonic dependency between input and output parameter.

Sensitivity analysis is completed for the following input parameters and ranges: initial contingency size (lines) $c_i \in [1, 200]$, maximum generation imbalance $\delta G_{\max} \in [0.0, 0.5]$, UVLS trigger voltage (p.u.) $U_{\text{UVLS}} \in [0.80, 0.95]$, maximum block-wise load shedding $\delta P_{\text{ls,max}} \in [0.05, 1.00]$, and maximum number of load shedding blocks $(\delta P_{\text{ls,max}})/(\delta P_{\text{ls}}) \in [1, 10]$. The output parameters are the indicators and Φ and Λ metrics introduced in Section III-E. Simulation results are obtained from the summer 2004 peak Polish power system containing 2736 buses and 3504 lines [32]. The network has a total generation capacity of 28.9 GW and a total demand of 18.1 GW. Reactive power capacity of the generators in the test case has been relaxed to +80% and −40% of the maximum active power output. This relaxation is purely to prevent the otherwise almost always instantaneous occurrence of voltage collapses due to excessively stringent reactive power limits. FAST was performed using the GSAT for MATLAB [39]. A sample size of 10 000 was sufficient for sensitivities to converge. The resulting sensitivities are shown in Fig. 9.

Initial contingency size has the largest impact on lost load, lost lines, and lost buses. The impact on lost generators is negligible. The Spearman coefficient reveals very strong positive correlation (coefficient is larger than +0.8) between initial contingency and lost load, lost lines, and lost buses. Increasing initial contingency size, thus, leads to larger and faster loss of load, lines, and buses.

Maximum generation imbalance only has a significant impact on lost generators. The Spearman coefficient reveals very strong negative correlation (coefficient is less than −0.8). Increasing maximum generation imbalance, thus, leads to less and slower loss of generators.

UVLS trigger voltage has no significant first-order impact. Maximum block-wise load shedding and number of load shedding blocks have a slight impact on lost generators. The Spearman coefficient reveals moderate negative correlation (coefficient between −0.6 and −0.4) of the number of load shedding blocks with Φ and Λ. A small number of load shedding blocks increases the load shedding per block, which leads to more rapid load shedding. This rapid load shedding causes generation imbalances and increases loss of generators.

V. Comparison to Historical Cascades

After the description of AC-CFM, its internal validation and sensitivity analysis in the previous sections, model outputs are now compared to historical cascades. According to the IEEE PES working group on cascading failures, a model must not necessarily exactly reproduce historical cascades, because the stochastic nature of the processes involved in cascades needs to be considered [3]. However, historical cascades show statistical behavior and distinctive patterns. The most important patterns are an acceleration of cascade propagation [12], [40], and a heavy-tailed distribution of blackout sizes [3], [41], [42]. A comparison and validation of statistical properties of simulations against historical data are, thus, feasible even if data are obtained from different networks and absolute values differ. Showing that historical and simulated cascades follow the same statistics

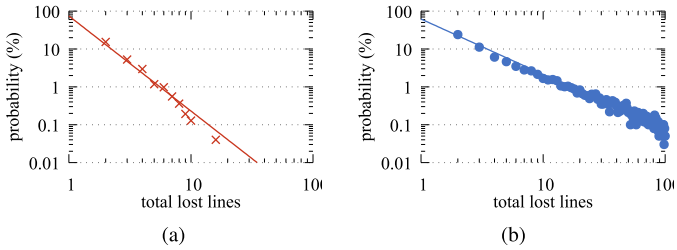

Fig. 10. Probability distribution of total lost lines. Dashed and solid lines show the Zipf distributions obtained from fitting. (a) Historical [12]. (b) AC-CFM.

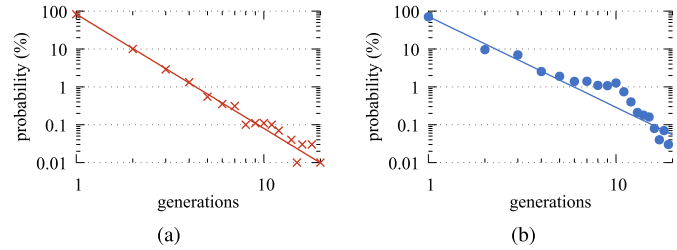

Fig. 11. Probability distribution of generations. Dashed and solid lines show the Zipf distributions obtained from fitting. (a) Historical [45]. (b) AC-CFM.

indicate that the model captures important features of cascading failures.

A. Network and Initial Contingency Set

The historical statistics used in this study are the records of lost load reported by the NERC Disturbance Analysis Working Group over a period of 22 years, and statistics derived from transmission line outage data reported by a North American utility over a period of 12.4 years [43]. In a static model, it is relatively easy to express causalities between individual line outages and distinguish between cascade generations, but it is challenging when looking at historical outage data. The process described in [12] uses time differences between line outages to group individual line outages into cascades and generations. The dataset contains 589 lines and 10 512 outages, grouped into 6316 cascades.

Historical data are compared to statistical properties of simulations obtained from the 2736-bus Polish system, which has already been used in Section IV. The network has been chosen because it is an established test case, publicly available, and large enough to observe cascading effects.

The size of initial contingencies in historical cascades usually follows a Zipf distribution [12]. In order to generate a comparable dataset from AC-CFM, an initial contingency set is created, containing 10 000 scenarios of random line combinations with a Zipf-distributed contingency size.

B. Model Input Parameters

The initial values of the model input parameters are $\delta G_{\max} = 15\%$, $U_{\mathrm{UVLS}} = 0.95$ p.u., $\delta P_{\mathrm{ls}} = 5\%$, and $\delta P_{\mathrm{ls,max}} = 25\%$. Values have been chosen based on the sensitivity study completed in Section IV and established protection settings for UFLS and UVLS [44]. The dispatch overhead $\delta G_{\mathrm{overhead}} = 10\%$ relates to reported transmission and distribution losses. Expert judgment or additional studies may be required to adequately set these values on a per-network basis.

C. Propagation Characteristics

The probability distributions of total lost lines caused by the initial contingency set as well as the data obtained from the historical dataset follow a Zipf distribution (see Fig. 10). Absolute probabilities, and subsequently the slope of the Zipf distributions, differ as these are network-specific and depend on the initial contingency set. Zipf distributions can also be found for the number of generations in the cascades (see Fig. 11). The matching statistics of historical and simulated line outages is

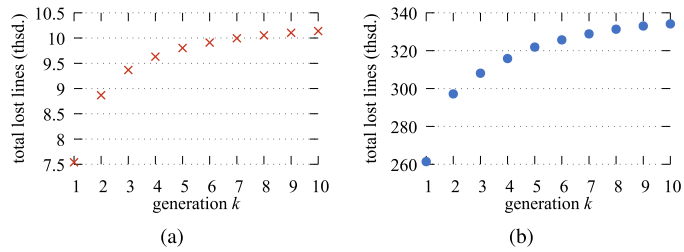

Fig. 12. Total number of lost lines for each generation. Modeled data are accumulated over 10 000 cascades. Historical data are taken from [12] and accumulated over 6316 cascades. (a) Historical [12]. (b) AC-CFM.

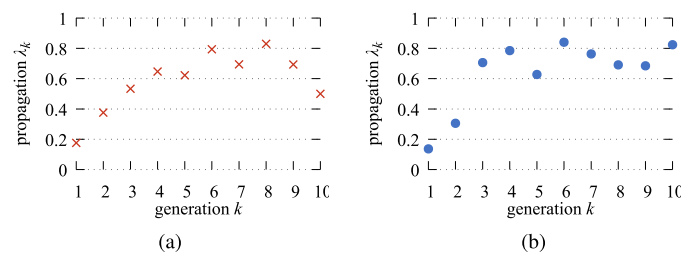

Fig. 13. Mean propagation λ_k for each generation. (a) Historical [12]. (b) AC-CFM.

a first indicator for the model capturing important features of cascading failures.

Next, the propagation of cascades over multiple generations is investigated. Fig. 12 shows the total accumulated number of lost lines at each generation, obtained from both AC-CFM and historical data. Historical data are only available for up to ten generations. The number of lost lines is significantly larger for AC-CFM dataset, because the underlying network contains more lines as discussed in Section V-A. However, it can be seen that for both datasets, the number of lost lines increases significantly during the first cascade generations and saturates after approximately the 10th generation.

Historical cascades show a distinctive acceleration during the initial generations [12], [40]. This is further analyzed by calculating the propagation λ_k, which quantifies the average tendency for the cascade to propagate from generation $k-1$ to generation k and is defined as $\lambda_k = Z_k/Z_{k-1}$ [12], where Z_k and Z_{k-1} are the number of lost lines in generation k and $k-1$, respectively. For historical cascades, the propagation λ_k increases during the first generations and then levels off [see Fig. 13(a)]. A later drop in propagation toward the end of cascades is not shown. The same trend is found for the propagation of cascades simulated with AC-CFM [see Fig. 13(b)]. For generations beyond 7, the

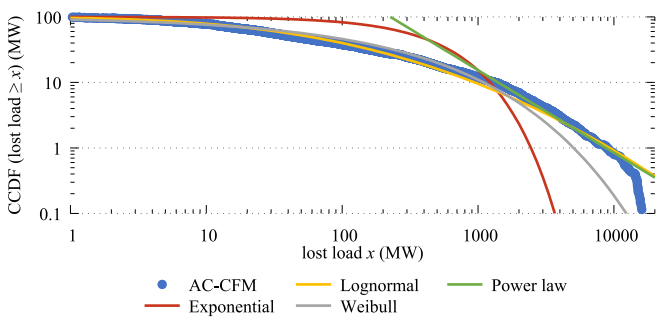

Fig. 14. CCDF of lost load as calculated by AC-CFM, including only contingencies that led to outages, and fitted probability distributions.

data become noisy as there are not many cascades with this number of generations. It should be noted that the way in which the individual lost lines are grouped into generations is different for historical and modeled data, but the distinctive increase in propagation supports the validation of AC-CFM.

D. Impact Characteristics

Blackout sizes, commonly expressed by the number of customers affected or the lost load caused, are usually presented as a complementary cumulative distribution function (CCDF) [14], [41], [42]. Analyses of historical data from the U.S. [41] and Europe [42] show that the CCDF of blackout sizes follows power law behavior in the tail with cut-off. The heavy tail present in the power law distribution indicates that larger blackouts are more likely than expected following conventional risk analysis [3]. Fig. 14 shows the CCDF of lost load caused by the given initial contingency set. The results are compared to fits to exponential, Weibull, lognormal, and power law with cut-off distributions. The cut-off frequency $x_{\min}$ is determined by a goodness-of-fit estimation based on the Kolmogorov–Smirnov test, as described in [46].

The CCDF drops slower than the exponential distribution, making it heavy-tailed, and shows three distinctive regions. For lost load $x < 1000$ MW, the shape resembles a lognormal or Weibull distribution. For lost load $1000 < x < 10000$, the CCDF shows power law behavior. For lost load $x > 10000$ MW, the CCDF drops abruptly. This is due to the lost load being close to the total load of the network, which amplifies border effects and stresses the model beyond its validity.

E. Summary of Comparison to Historical Cascades

The comparisons of the propagation and impact characteristics show that calculations by AC-CFM show the same distinctive pattern that can be observed in historical outage data. In particular

1) The number of lost lines and the number of generations follow Zipf distributions as reported in [12] and [45].
2) The propagation increases during the first generations and saturates as reported in [12].
3) The lost load calculated by AC-CFM follow a power law distribution as reported in [41] and [42].

While matching statistics do not prove the validity of AC-CFM, this analysis provides a positive indication of the model capturing important features of cascading failures.

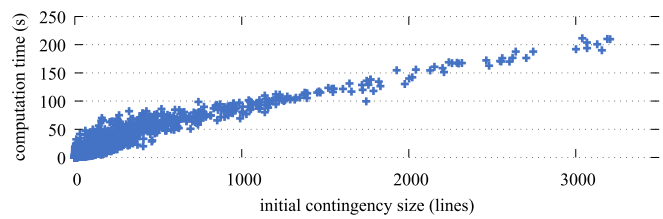

Fig. 15. Computation time analysis.

VI. Performance and Convergence

The model was run on a machine with an Intel Xeon E5-2620 CPU and 32 GB RAM. When calculating multiple scenarios, AC-CFM can be parallelized in order to make use of all processor cores. The computation time for modeling the 10 000 scenarios in Section V in the 2736-bus Polish system was 2.25 h. Fig. 15 shows the computation time per scenario and reveals an approximately proportional dependency to the size of the initial contingency. The correlation coefficient is 0.94, indicating a strong positive relationship. Approximately proportional behavior can also be found for the number of PFs to be calculated and initial contingency size (correlation coefficient 0.99). Within the 10 000 scenarios, AC-CFM calculated 210 205 PFs. Out of these, the PF did not converge in 11 745 cases (5.6%), and VCLS was applied. Nonconvergence of PF showed no correlation with island size. In 1379 cases (0.7%), VCLS failed and the island was tripped. In 95% of cases in which VCLS failed, the island had a size of 30 or less nodes. This demonstrates that VCLS successfully solves convergence issues and that tripping in case of nonconvergence mainly affects small islands with a lack of reactive power support.

VII. Cross-Validation to Existing AC Model

In this section, the computational cost and results obtained from AC-CFM are compared to ACSimSep [22], an established ac-based cascading failure model. Comparison is done as a cross-validation of models as well as to highlight similarities and differences between the approaches. ACSimSep models tripping of overloaded of lines and rebalancing of PFs by shedding loads or generators. ACSimSep ignores reactive power limits or undervoltage protection, meaning it does not capture the physical capability of a network and the whole extent of cascading failures. In case of nonconverging PFs, ACSimSep uses sensitivity factors to identify the load buses that most effectively move the network into a solvable region.

Both models are applied to the previously introduced network and initial contingency set of Section V. Modeling 10 000 scenarios on the machine presented in Section VI took 2.25 h for AC-CFM and 1.4 h for ACSimSep. Computation time is, thus, on a similar time scale, however, AC-CFM being somewhat slower than ACSimSep. Time differences can be mainly attributed to the more detailed modeling of undervoltage protection in AC-CFM, with 81.8% of scenarios in which UVLS or VCLS are involved leading to a time difference of more than one second. In 75% of scenarios, AC-CFM is not more than 0.57 s slower than ACSimSep.

The mean difference (95% confidence limits) of lost load calculated by AC-CFM minus ACSimSep is 0.09% (−8.34%, 8.16%). Looking at each scenario individually, AC-CFM tends

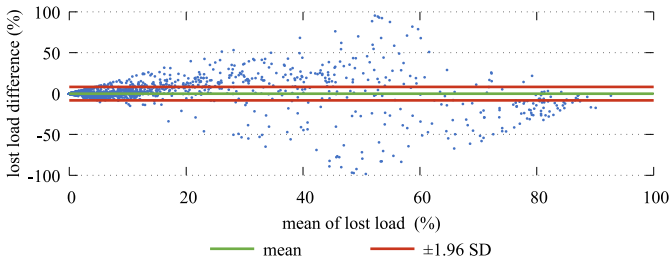

Fig. 16. Mean-difference plot comparing lost load calculated by AC-CFM and ACSimSep.

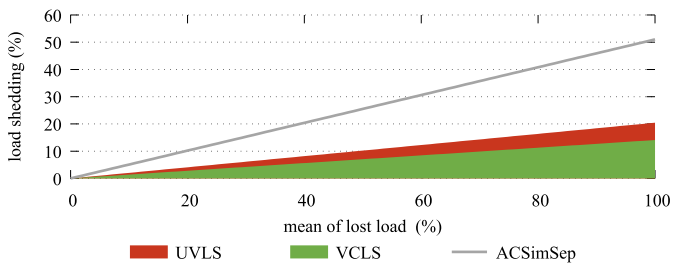

Fig. 17. Linear regressions of load shedding due to nonconverging PFs in AC-CFM and ACSimSep.

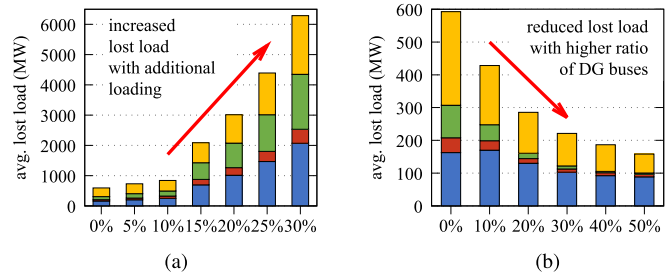

Fig. 18. Causes of lost load: UFLS (blue), UVLS (red), VCLS (green), and tripped buses (yellow). (a) Additional loading. (b) Ratio of DG buses.

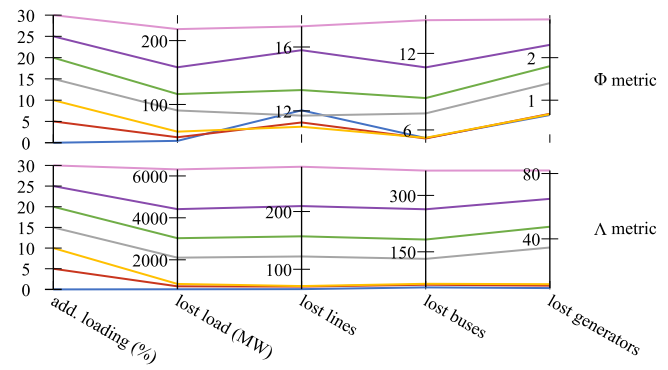

Fig. 19. Average resilience metrics depending on additional loading.

to give larger (smaller) lost loads than ACSimSep for scenarios with a small (large) mean lost load (see Fig. 16).

This behavior can be related to two main differences between the models. First, modeling of UVLS and O/UXL in AC-CFM adds further constraints on the network by requiring that voltage and reactive power limits are maintained. These mechanisms increase the lost load for most of the scenarios. Second, VCLS, which is used by AC-CFM to obtain a solvable PF in case of nonconvergence, is in most cases more efficient than the sensitivity-based approach of ACSimSep, meaning that AC-CFM requires less load shedding in order to make the PF solvable again than ACSimSep (see Fig. 17). This reduces the lost load calculated by AC-CFM particularly for larger failures, in which nonconverging PFs become more likely. As discussed in Section III-B, the reaction of a model to nonconverging PFs must be cautious, because an overshooting reaction, i.e., excessive load shedding, may prevent the revelation of underlying voltage issues.

VCLS can leave the network in a state with undervoltages at some buses. This often causes subsequent UVLS, although UVLS can also be caused by islanding, loss of generators or lines. In general, the amount of UVLS increases for cascades with larger lost load, but the combined load shedding by VCLS and UVLS in AC-CFM is still significantly less than load shedding due to nonconvergence in ACSimSep.

Summarizing, cross-validation of AC-CFM with ACSimSep has shown that the approach taken in AC-CFM to obtain a solvable PF in case of nonconvergence is more efficient, and it does not prevent the identification of subsequent undervoltage issues. While the overall lost load as calculated by both models is in most cases comparable, AC-CFM, thus, provides deeper understanding of the impact of cascading failures.

VIII. Applications for AC-CFM

AC-CFM allows for a wide range of studies of resilience to cascading failures. This section provides an insight into possible analyses that can be undertaken, however, the application of the model is not limited to these fields of study. The analyses are performed using the previously introduced 2736-bus Polish network. Section V-A lists the model input parameters and describes the initial contingency set with 10 000 contingencies.

A. Network Loading

A key question in resilience studies is how resilience changes with increasing network loading due to additional loads and generation. Beginning with the default loading, all loads are increased in steps of 5%. The generation capacity is adjusted likewise. Until an additional loading of 10%, the average lost load does not increase significantly [see Fig. 18(a)]. From an additional loading of 15% on, an approximately linear increase of average load shedding can be observed. Lost load is caused by UFLS, UVLS, VCLS, and tripped buses, i.e., buses that become part of an island without generation or insufficient ramping capability. AC-CFM can, thus, be used to determine the critical loading, beyond which mean lost load sharply increases. The existence of such a critical loading has been previously shown in other works, such as [47]. The UK National Infrastructure Commission emphasizes the need for thorough stress testing and determination of system breaking points, as it can be performed by AC-CFM, in its report on resilient infrastructure systems [48].

For further understanding of this behavior, the mean values of the Φ and Λ metrics from the $\Phi\Lambda E\Pi$ resilience metric framework are calculated. While metrics do not change for additional loading of up to 10%, both metrics for all indicators increase significantly from an additional loading of 15% on (see Fig. 19).

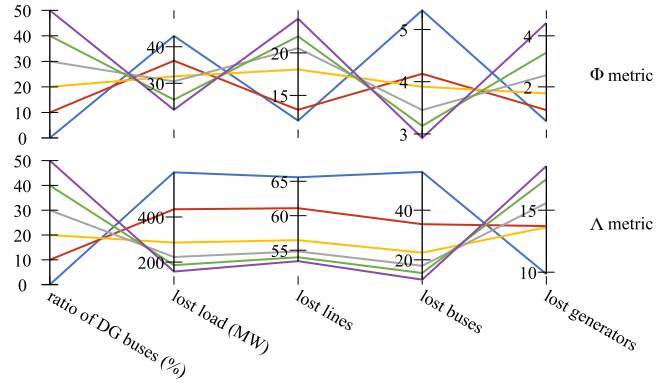

Fig. 20. Average resilience metrics depending on ratio of DG buses.

This means that loads, lines, buses, and generators are lost more and faster with increasing network loading. Additional loads can, thus, only be connected up to a certain loading level without significantly reducing resilience.

Following the results, critical loading is governed by the physical limitations of the network and its protection settings. For instance, adding inertia to the network, thus increasing $\delta G_{\max}$, or deploying shunt devices for voltage support are some of the measures that can relax the physical limitations. Easing of protection settings can delay the activation of protection mechanisms, but might trigger subsequent damage to the system and must be done carefully. Preventive measures building on the capabilities of a modern smart grid, such as defensive or corrective islanding, can also improve critical loading of networks [7].

B. Distributed Generation

A further trend is the increasing amount of distributed generation (DG) connected to the network, whilst large and conventional generators are being disconnected. To model this, the initial 2736-bus Polish network is modified by adding DG with a capacity of 10 MW each, a typical maximum size for generators connected to the distribution system [49], to a certain ratio of DG buses. In a real network, DG can be accumulations of a number of small-scale generators connected to the same bus. It is assumed that DG is grid-forming. The generation capacity of conventional generators is downsized so that the overall generation capacity does not change. The model is applied to various ratios of DG buses, and the mean values of the Φ and Λ resilience metrics are calculated. With increasing ratio of DG buses from 0% to 50%, lost load decreases approximately exponentially [see Fig. 18(b)]. Particularly the amount of UVLS, VCLS, and lost load due to tripped buses is reduced, while the reduction in UFLS is not as significant.

This is further analyzed by calculating the mean values of the Φ and Λ metrics from the $\Phi\Lambda E\Pi$ resilience metric framework. With increasing ratio of DG buses, loads, and buses are lost less and slower (see Fig. 20). Larger ratios of DG buses also decrease the number of lines lost, but lines are lost faster. Generators are lost more and faster, however, this is mainly controlled by the coordination of OFGS.

Increasing the ratio of DG can, thus, improve power network resilience and limit the lost load caused by cascading failures in several ways, if it is connected and controlled adequately. First, a larger number of DG decreases the number of buses that are part of islands formed during a cascade and lack generation capacity, and are, thus, tripped. Second, DG stabilizes bus voltages and reduces the amount of UVLS. This is in line with previous findings in the literature, such as [50].

However, recent cases such as the 2019 blackout in the United Kingdom have shown that large amounts of DG in combination with inadequate protection settings can increase the risk of blackouts and, thus, reduce power network resilience [51]. Deployment of DG, hence, requires additional protection mechanisms to particularly deal with large frequency fluctuations and loss of mains. Such mechanisms could be added to the model at a later stage.

C. Key Findings of AC-CFM for Resilience Improvements

AC-CFM can facilitate key improvements of power network resilience in three ways. First, the model provides insights into how cascading failures propagate within power networks, for instance, by providing visualizations of cascades (see Section III-D). It highlights the need for and contribution of various protection mechanisms in cascading failures (see Sections VIII-A and VIII-B). The capability of AC-CFM to handle large contingencies, shown in Section V, is vital for such investigations. Second, by using cascade visualizations, the model can identify network components, such as lines or buses that are involved in large cascades and the type of issues that arise, such as undervoltages or overloads. Thus, improvement strategies can be developed, for instance, for the location of shunt devices or additional transmission line capacity. Third, the model can assess the resilience of a power network after such improvement strategies have been developed, particularly for future network scenarios such as increased loading or deployment of DG.

IX. Conclusion

This article presented a novel AC-CFM specifically designed for resilience analysis of power networks. The model incorporates dynamic phenomena and protection mechanisms in a static representation, giving insights into how protection mechanisms interact in the propagation of cascading failures, whilst being computationally fast. Nonconverging PFs are specifically addressed by the model using established OPF solvers to make AC-CFM stable even for very large contingency sizes, which are of crucial interest in power network resilience.

The model was thoroughly validated following the recommendations by the IEEE PES working group on cascading failures. An internal validation provided dynamic simulations of the implemented protection mechanisms and their impact on power networks. A comparison to statistics extracted from historical outages in Europe and the U.S. showed that the model matches the statistics in terms of propagation characteristics and heavy-tail behavior observed in real cascades. A sensitivity study of the input parameters revealed that cascading failures are, besides network topology, mainly governed by the initial contingency size and maximum generation imbalance in a network. A cross-validation comparing AC-CFM to an existing ac-based cascading failure model showed that AC-CFM provides matching results in terms of lost load, however, it handles nonconverging PFs in a more efficient manner and models undervoltage issues to a greater detail. This adds to the understanding of how cascading failures propagate and helps mitigating large and wide-spread blackouts. Case studies demonstrating possible applications of AC-CFM showed that the model seamlessly links to established

resilience metric frameworks such as ΦΛΕΠ, which simplifies its integration into existing research and enhances comparability. AC-CFM will be made available to researchers via Github as a powerful and valuable tool for resilience analysis of power networks.

Appendix
Exemplary Model Output

The IEEE 39-bus test network, initial fault of line 4–14.

```
Demand increased by 0.1% (limit is 15.0%) and genera-
  tion capacity is met. Distribute slack generation.
Exceeded line ratings: 6-11

Demand increased by 0.5% (limit is 15.0%) and genera-
  tion capacity is met. Distribute slack generation.
Q outside limits at generators at buses 34
Exceeded line ratings: 3-4 3-18 10-13 13-14 14-15
  16-17 17-18

3 islands and 2 isolated nodes detected
Island: [ 1 2 3... 9 17 25 26 27... 31 37 38 39 ]
  Demand increased by 20.9% (limit is 15.0%) or gene-
  ration capacity is not met.
  Perform underfrequency load shedding of 12.2%.

  Q outside limits at generators at buses 31 39
  Voltage outside limits at buses 4 7 8
  Undervoltage load shedding applied at buses 4 7 8
  Exceeded line ratings: 1-2 8-9 9-39

  3 islands and 1 isolated nodes detected
  Island: [ 2 3 17 25 26 27... 30 37 38 ]
    Demand decreased by 42.6% (limit is 15.0%).
       Tripping 2 smallest generators.

    Loads shed (22.54%) due to voltage collapse at
      buses 26 29

    Demand increased by 0.0% (limit is 15.0%) and ge-
      neration capacity is met. Distribute slack ge-
      neration.
    Exceeded line ratings: 2-25 2-30

    2 islands and 1 isolated nodes detected
    Island: [ 17 25 26 27 28 29 37 38 ]
      No generation available.

    Island: [ 2 3 ]
      No generation available.

    Island: [ 30 ]
      Demand decreased by 100.0% (limit is 15.0%).
      Tripping 1 smallest generators.

  Island: [ 4 5 6 7 8 31 ]
    Demand increased by 400.4% (limit is 15.0%) or
      generation capacity is not met. Perform under-
      frequency load shedding of 79.0%.

  Island: [ 1 39 ]
    Demand decreased by 4.0% (limit is 15.0%).
      Distribute slack generation.

  Island: [ 9 ]
    No generation available.

Island: [ 15 16 19 20 21... 24 33 34 35 36 ]
  Demand decreased by 8.4% (limit is 15.0%).
    Distribute slack generation.

Island: [ 10 11 12 13 32 ]
  Demand decreased by 98.7% (limit is 15.0%).
    Tripping 1 smallest generators.

  No generation available.

Island: [ 14 ]
  No generation available.

Island: [ 18 ]
  No generation available.

Cascade halted. Elapsed time: 6.80 s
Total load shedding: 45.05%
Load shedding UFLS: 20.97%
Load shedding UVLS: 0.88%
Load shedding VCLS: 4.61%
Load shedding non-converging OPF: 0.00%
Load shedding tripped: 18.59%
```

References

[1] M. Panteli and P. Mancarella, "Modeling and evaluating the resilience of critical electrical power infrastructure to extreme weather events," *IEEE Syst. J.*, vol. 11, no. 3, pp. 1733–1742, Sep. 2017.

[2] Y. Lin, Z. Bie, and A. Qiu, "A review of key strategies in realizing power system resilience," *Global Energy Interconnection*, vol. 1, no. 1, pp. 70–78, 2018.

[3] J. Bialek *et al.*, "Benchmarking and validation of cascading failure analysis tools," *IEEE Trans. Power Syst.*, vol. 31, no. 6, pp. 4887–4900, Nov. 2016.

[4] M. Vaiman *et al.*, "Risk assessment of cascading outages: Methodologies and challenges," *IEEE Trans. Power Syst.*, vol. 27, no. 2, pp. 631–641, May 2012.

[5] M. Panteli, D. N. Trakas, P. Mancarella, and N. D. Hatziargyriou, "Boosting the power grid resilience to extreme weather events using defensive islanding," *IEEE Trans. Smart Grid*, vol. 7, no. 6, pp. 2913–2922, Nov. 2016.

[6] Y. P. Fang, N. Pedroni, and E. Zio, "Comparing network-centric and power flow models for the optimal allocation of link capacities in a cascade-resilient power transmission network," *IEEE Syst. J.*, vol. 11, no. 3, pp. 1632–1643, Sep. 2017.

[7] M. Noebels and M. Panteli, "Assessing the Effect of Preventive Islanding on Power Grid Resilience," in *Proc. IEEE Milan PowerTech.*, 2019, pp. 1–6.

[8] H. Guo, C. Zheng, H. H. C. Iu, and T. Fernando, "A critical review of cascading failure analysis and modeling of power system," *Renew. Sustain. Energy Rev.*, vol. 80, pp. 9–22, 2017.

[9] P. Crucitti, V. Latora, and M. Marchiori, "Model for cascading failures in complex networks," *Phys. Rev. E - Statist. Phys., Plasmas, Fluids, Related Interdisciplinary Topics*, vol. 69, no. 4, pp. 1–4, 2004.

[10] X. Zhang, C. Zhan, and C. K. Tse, "Modeling the dynamics of cascading failures in power systems," *IEEE J. Emerg. Sel. Topics Circuits Syst.*, vol. 7, no. 2, pp. 192–204, Jun. 2017.

[11] I. Dobson, B. A. Carreras, and D. E. Newman, "A loading-dependent model of probabilistic cascading failure," *Probab. Eng. Informational Sci.*, vol. 19, no. 1, pp. 15–32, 2005.

[12] I. Dobson, "Estimating the propagation and extent of cascading line outages from utility data with a branching process," *IEEE Trans. Power Syst.*, vol. 27, no. 4, pp. 2146–2155, Nov. 2012.

[13] J. Kim, K. R. Wierzbicki, I. Dobson, and R. C. Hardiman, "Estimating propagation and distribution of load shed in simulations of cascading blackouts," *IEEE Syst. J.*, vol. 6, no. 3, pp. 548–557, Sep. 2012.

[14] B. A. Carreras, V. E. Lynch, I. Dobson, and D. E. Newman, "Critical points and transitions in an electric power transmission model for cascading failure blackouts," *Chaos*, vol. 12, no. 4, pp. 985–994, 2002.

[15] M. A. Rios, D. S. Kirschen, D. Jayaweera, D. P. Nedic, and R. N. Allan, "Value of security: Modeling time-dependent phenomena and weather conditions," *IEEE Trans. Power Syst.*, vol. 17, no. 3, pp. 543–548, Aug. 2002.

[16] M. J. Eppstein and P. D. Hines, "A "random chemistry" algorithm for identifying collections of multiple contingencies that initiate cascading failure," *IEEE Trans. Power Syst.*, vol. 27, no. 3, pp. 1698–1705, Aug. 2012.

[17] H. Sabouhi, A. Doroudi, M. Fotuhi-Firuzabad, and M. Bashiri, "Electrical power system resilience assessment: A comprehensive approach," *IEEE Syst. J.*, vol. 14, no. 2, pp. 2643–2652, Jun. 2020.

[18] S. Yang, W. Chen, X. Zhang, C. Liang, H. Wang, and W. Cui, "A graph-based model for transmission network vulnerability analysis," *IEEE Syst. J.*, vol. 14, no. 1, pp. 1447–1456, Mar. 2020.

[19] A. Muir and J. Lopatto, "Final report on the August 14, 2003 blackout in the United States and Canada: Causes and recommendations," U.S.-Canada Power System Outage Task Force, Rep. AR-1165, 2004.

[20] J. M. Ordacgi Filho, "Brazilian blackout 2009: Blackout watch," in *Proc. PAC World Mag.*, Mar. 2010, pp. 36–37.

[21] H. Cetinay, S. Soltan, F. A. Kuipers, G. Zussman, and P. Van Mieghem, "Analyzing cascading failures in power grids under the AC and DC power flow models," *Perform. Eval. Rev.*, vol. 45, no. 3, pp. 198–203, 2018.
[22] P. D. Hines and P. Rezaei, "Cascading failures in power systems," in *Smart Grid Handbook*, vol. 1, Hoboken, NJ: Wiley, 2016.
[23] G. Fu *et al.*, "Integrated approach to assess the resilience of future electricity infrastructure networks to climate hazards," *IEEE Syst. J.*, vol. 12, no. 4, pp. 3169–3180, Dec. 2018.
[24] S. Poudel, A. Dubey, and A. Bose, "Risk-based probabilistic quantification of power distribution system operational resilience," *IEEE Syst. J.*, vol. 14, no. 3, pp. 3506–3517, Sep. 2020.
[25] D. A. Reed, K. C. Kapur, and R. D. Christie, "Methodology for assessing the resilience of networked infrastructure," *IEEE Syst. J.*, vol. 3, no. 2, pp. 174–180, Jun. 2009.
[26] F. H. Jufri, V. Widiputra, and J. Jung, "State-of-the-art review on power grid resilience to extreme weather events: Definitions, frameworks, quantitative assessment methodologies, and enhancement strategies," *Appl. Energy*, vol. 239, pp. 1049–1065, Feb. 2019.
[27] M. Panteli, P. Mancarella, D. N. Trakas, E. Kyriakides, and N. D. Hatziargyriou, "Metrics and quantification of operational and infrastructure resilience in power systems," *IEEE Trans. Power Syst.*, vol. 32, no. 6, pp. 4732–4742, Nov. 2017.
[28] M. Braun, C. Hachmann, and J. Haack, "Blackouts, restoration, and islanding," *IEEE Power Energy Mag.*, vol. 18, no. 4, pp. 54–63, Jul./Aug. 2020.
[29] J. Zhao, H. Wang, Y. Liu, Q. Wu, Z. Wang, and Y. Liu, "Coordinated restoration of transmission and distribution system using decentralized scheme," *IEEE Trans. Power Syst.*, vol. 34, no. 5, pp. 3428–3442, Sep. 2019.
[30] M. R. Kelly-Gorham, P. D. Hines, K. Zhou, and I. Dobson, "Using historical utility outage data to compute overall transmission grid resilience," *Electric Power Systems Research*, vol. 189, no. 106676, pp. 1–7, Dec. 2020.
[31] W. Liu, J. Zhan, C. Y. Chung, and L. Sun, "Availability assessment based case-sensitive power system restoration strategy," *IEEE Trans. Power Syst.*, vol. 35, no. 2, pp. 1432–1445, Mar. 2020.
[32] R. D. Zimmerman, C. E. Murillo-Sanchez, and R. J. Thomas, "MATPOWER: Steady-state operations, planning, and analysis tools for power systems research and education," *IEEE Trans. Power Syst.*, vol. 26, no. 1, pp. 12–19, Feb. 2011.
[33] J. Song, E. Cotilla-Sanchez, G. Ghanavati, and P. D. Hines, "Dynamic modeling of cascading failure in power systems," *IEEE Trans. Power Syst.*, vol. 31, no. 3, pp. 2085–2095, May 2016.
[34] S. Mei, Y. Ni, G. Wang, and S. Wu, "A study of self-organized criticality of power system under cascading failures based on AC-OPF with voltage stability margin," *IEEE Trans. Power Syst.*, vol. 23, no. 4, pp. 1719–1726, Nov. 2008.
[35] Q. Chen and L. Mili, "Composite power system vulnerability evaluation to cascading failures using importance sampling and antithetic variates," *IEEE Trans. Power Syst.*, vol. 28, no. 3, pp. 2321–2330, Aug. 2013.
[36] A. Wächter and L. T. Biegler, "On the implementation of an interior-point filter line-search algorithm for large-scale nonlinear programming," *Math. Program.*, vol. 106, no. 1, pp. 25–57, 2006.
[37] North American Electric Reliability Corporation, "Automatic Underfrequency Load Shedding (PRC-006-3)," Atlanta, GA, USA, 2017.
[38] G. J. McRae, J. W. Tilden, and J. H. Seinfel, "Global sensitivity analysis—A computational implementation of the fourier amplitude sensitivity test (FAST)," *Comput. Chem. Eng.*, vol. 6, no. 1, pp. 15–25, 1982.
[39] F. Cannavó, "Sensitivity analysis for volcanic source modeling quality assessment and model selection," *Comput. Geosci.*, vol. 44, pp. 52–59, 2012.
[40] I. Dobson, B. A. Carreras, and D. E. Newman, "Branching process models for the exponentially increasing portions of cascading failure blackouts," in *Proc. Annu. Hawaii Int. Conf. Syst. Sci.*, pp. 1–10, 2005.
[41] P. Hines, J. Apt, and S. Talukdar, "Trends in the history of large blackouts in the United States," in *Proc. IEEE Power Energy Soc. Gen. Meeting Convers. Deliv. Elect. Energy 21st Century*, pp. 1–8, vol. 15213, 2008.
[42] M. Rosas-Casals and R. Solé, "Analysis of major failures in Europe's power grid," *Int. J. Elect. Power Energy Syst.*, vol. 33, no. 3, pp. 805–808, 2011.
[43] "Bonneville power administration transmission services operations and reliability reports," BPA. 2020. [Online]. Available: https://transmission.bpa.gov/Business/Operations/Outages/
[44] R. M. Larik, M. W. Mustafa, and M. N. Aman, "A critical review of the state-of-art schemes for under voltage load shedding," *Int. Trans. Elect. Energy Syst.*, vol. 29, no. 5, pp. 1–26, 2019.
[45] I. Dobson, "Finding a Zipf distribution and cascading propagation metric in utility line outage data," 2018, *arXiv:1808.08434*.
[46] A. Clauset, C. R. Shalizi, and M. E. Newman, "Power-law distributions in empirical data," *SIAM Rev.*, vol. 51, no. 4, pp. 661–703, 2009.
[47] I. Dobson, B. A. Carreras, V. E. Lynch, and D. E. Newman, "Complex systems analysis of series of blackouts: Cascading failure, critical points, and self-organization," *Chaos*, vol. 17, no. 026103, pp. 1–13, Jun. 2007.
[48] National Infrastructure Commission, "Anticipate, react, recover. Resilient infrastructure systems," London, U.K., 2020.
[49] R. C. Dugan and T. E. McDermott, "Distributed generation," *IEEE Ind. Appl. Mag.*, vol. 8, no. 2, pp. 19–25, Mar./Apr. 2002.
[50] A. Camacho, M. Castilla, J. Miret, L. G. De Vicuna, and G. L. Miguel Andres, "Control strategy for distribution generation inverters to maximize the voltage support in the lowest phase during voltage sags," *IEEE Trans. Ind. Electron.*, vol. 65, no. 3, pp. 2346–2355, Mar. 2018.
[51] National Grid ESO, "Technical Report on the events of 9 Aug. 2019," Warwick, U.K., 2019.

Matthias Noebels (Student Member, IEEE) received the M.Sc. degree in physics from the University of Konstanz, Konstanz, Germany, in 2015. He is currently working toward the Ph.D. degree in electrical engineering with the Centre for Doctoral Training in Power Networks, The University of Manchester, Manchester, U.K.

His expertise lies in resilience analysis of power networks as well as developing strategies that can enhance resilience in case of natural hazards such as extreme weather.

Robin Preece (Senior Member, IEEE) received the B.Eng. degree in electrical and electronic engineering and Ph.D. degree in power systems engineering from The University of Manchester, Manchester, U.K., in 2009 and 2013, respectively.

He is currently a Senior Lecturer in Future Power Systems with the Department of Electrical and Electronic Engineering, The University of Manchester. His research interests focus on the stability and operation of future power systems.

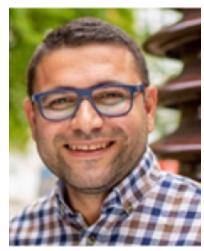

Mathaios Panteli (Senior Member, IEEE) received the M.Eng. degree in electrical and computer engineering from the Aristotle University of Thessaloniki, Thessaloniki, Greece, in 2009, and the Ph.D. degree in electrical power engineering from The University of Manchester, Manchester, U.K., in 2013.

He is currently an Assistant Professor with the Power and Energy Division, The University Manchester. His main research interests include analysis and prevention of blackouts, risk and resilience assessment of future low-carbon power systems and integrated modelling of codependent critical infrastructures.

Dr. Panteli is an IET Chartered Engineer (C.Eng.), the Co-Chair of the CIGRE WG C4.47 Power System Resilience and an active member of multiple IEEE working groups. He is also the recipient of the prestigious 2018 Newton Prize.